position, compatible with the endoprotease specificity of TPPII. Most MHC class I–binding peptides have hydrophobic COOH-terminal amino acids generated by proteasomes. However, we have observed occasional endoproteolytic cleavage after hydrophobic amino acids by TPPII as well (*13*). Limited peptide supply may also be compensated by protection of peptides by increased levels of heat shock proteins. In combination, these factors may account for the partially maintained MHC class I expression in LLL(VS)-adapted cells (*2*) and in lactacystin-adapted cells (*13*). Cell-cycle progression and degradation of ubiquitinated proteins appear to continue in the absence of normal proteasome function (*2*). What role TPPII plays in these processes is not yet clear. We envisage multiple compensatory mechanisms operating in cells with compromised proteasomal function.

References and Notes

1. O. Coux, K. Tanaka, A. L. Goldberg, *Annu. Rev. Biochem.* **65**, 801 (1996); A. Ciechanover and A. Schwartz, *Proc. Natl. Acad. Sci. U.S.A.* **95**, 2727 (1998); K. L. Rock *et al.*, *Cell* **78**, 761 (1994); V. J. Palombella, O. J. Rando, A. L. Goldberg, T. Maniatis, *ibid.*, p. 773; R. W. King, R. J. Deshaies, J.-M. Peters, M. W. Kirschner, *Science* **274**, 1652 (1996).
2. R. Glas, M. Bogyo, J. S. McMaster, M. Gaczynska, H. L. Ploegh, *Nature* **392**, 618 (1998).
3. Murine EL4 thymoma cells (8×10^9 to 1×10^{10} cells) were harvested and resuspended at a density of 3×10^7 cells per milliliter in imidazole buffer [20 mM imidazole-HCl (pH 6.8), 100 mM KCl, 20 mM EGTA, 2 mM $MgCl_2$, 10% sucrose, 1 mM adenosine triphosphate (ATP)] and lysed by freeze-thawing. The lysate was differentially centrifuged (15 min at 1500*g*, 15 min at 15,000*g*, 60 min at 100,000*g*, 3 hours at 100,000*g*), and the resulting pellet of HMW proteins was resuspended in 50 mM tris-HCl (pH 7.4), 20% glycerol, 5 mM $MgCl_2$, 0.5 mM β-mercaptoethanol, 1 mM ATP) and stored at −80°C. Samples of the resuspended material were separated on a Mono Q (HR16/10) anion-exchange column [buffer A: 20 mM Hepes (pH 7.2), 15% glycerol, 1 mM ATP; buffer B: 20 mM Hepes (pH 7.2), 15% glycerol, 1 M NaCl, 1 mM ATP] followed by gel filtration on a Superose 6-column [2 cm by 50 cm; elution buffer: 20 mM Hepes (pH 7.2), 100 mM NaCl, 15% glycerol, 1 mM ATP]. All purification steps were carried out at 4°C. Samples of collected fractions were used to measure hydrolysis of Suc-LLVY-AMC and AAF-AMC (*4*).
4. Peptidase assays were performed as described (*14*).
5. The protein was digested with trypsin in a 50 mM NH_4HCO_3, 5 mM $CaCl_2$ buffer containing 33% isotopically labeled $H_2{}^{18}O$. Peptides are isotopically labeled to 33% at their COOH-terminus, thereby allowing COOH-terminal fragments (y-ions) to be distinguished from other fragment ions by their specific $^{16}O/^{18}O$ isotopic distribution. The peptides were sequenced on a API III triple quadrupole instrument (PE-Sciex, Toronto, Canada) equipped with a nanoelectrospray source by differential scanning (M. Wilm, G. Neubauer, L. Taylor, A. Shevchenko, A. Bachi, in preparation).
6. B. Tomkinson, *Biochem. J.* **304**, 517 (1994).
7. C. Rose *et al.*, *Nature* **380**, 403 (1996).
8. R. M. Balöw, U. Ragnasson, Ö. Zetterqvist, *J. Biol. Chem.* **258**, 11622 (1983); R. M. Balöw, B. Tomkinson, U. Ragnarsson, Ö. Zetterqvist, *ibid.* **261**, 2409 (1986); E. Macpherson, B. Tomkinson, R. M. Balöw, S. Höglund, Ö. Zetterqvist, *Biochem. J.* **248**, 259 (1987).
9. J. Walz *et al.*, *J. Struct. Biol.* **121**, 19 (1998).
10. P. C. Ramos *et al.*, *Cell* **92**, 489 (1998).
11. T. Tamura *et al.*, *Science* **274**, 1385 (1996).
12. G. Fenteany *et al.*, *ibid.* **268**, 726 (1995).
13. E. Geier, K. Eichmann, G. Niedermann, data not shown.
14. G. Niedermann *et al.*, *Proc. Natl. Acad. Sci. U.S.A.* **93**, 8572 (1996).
15. H. Kirschke *et al.*, *Acta Biol. Med. Ger.* **36**, 185 (1977); T. Nishimura, A. Okitani, R. Katakai, H. Kato, *Eur. J. Biochem.* **137**, 23 (1983); F. Bermpohl, K. Löster, W. Reutter, O. Baum, *FEBS Lett.* **428**, 152 (1998).
16. S. Imajoh-Ohmi *et al.*, *Biochem. Biophys. Res. Commun.* **217**, 1070 (1995); X. Wang, H. Luo, H. Chen, W. Duguid, J. Wu, *J. Immunol.* **160**, 788 (1998).
17. M. Zhou, X. Wu, H. N. Ginsberg, *J. Biol. Chem.* **271**, 24769 (1996); K. T. Bush, A. L. Goldberg, S. K. Nigam, *ibid.* **272**, 9086 (1997); A. B. Meriin, V. L. Gabai, J. Yaglom, V. I. Shifrin, M. Y. Sherman, *ibid.* **273**, 6373 (1998).
18. N. Tamura, F. Lottspeich, W. Baumeister, T. Tamura, *Cell* **95**, 637 (1998).
19. A. H. Benham, M. Gromme, J. Neefjes, *J. Immunol.* **161**, 63 (1998).
20. For each time point, 6 ng of TPPII was incubated with 3 μg of synthetic peptide corresponding to the ovalbumin amino acids 37 to 77 at 37°C in a total volume of 100 μl of assay buffer [20 mM Hepes (pH 7.8), 1 mM EGTA, 0.5 mM EDTA, 5 mM $MgCl_2$, 0.5 mM 2-mercaptoethanol, 5% glycerol]. The analysis of peptide products was performed as described (*14*).

21. We thank S. Gaedicke for technical assistance, E. J. Corey for supplying lactacystin, K. Peters and A. Würch for helpful discussions, and I. Haidl for critical reading of the manuscript. Supported by a grant of the Deutsche Forschungsgemeinschaft (NI 368/2-1) to G.N.

15 September 1998; accepted 15 January 1999

Role of NADH Shuttle System in Glucose-Induced Activation of Mitochondrial Metabolism and Insulin Secretion

Kazuhiro Eto,[1] Yoshiharu Tsubamoto,[1] Yasuo Terauchi,[1] Takuya Sugiyama,[1] Takuya Kishimoto,[2] Noriko Takahashi,[1] Naoko Yamauchi,[3] Naoto Kubota,[1] Shigeo Murayama,[4] Toru Aizawa,[5] Yasuo Akanuma,[6] Shinichi Aizawa,[7] Haruo Kasai,[2] Yoshio Yazaki,[1] Takashi Kadowaki[1]*

Glucose metabolism in glycolysis and in mitochondria is pivotal to glucose-induced insulin secretion from pancreatic β cells. One or more factors derived from glycolysis other than pyruvate appear to be required for the generation of mitochondrial signals that lead to insulin secretion. The electrons of the glycolysis-derived reduced form of nicotinamide adenine dinucleotide (NADH) are transferred to mitochondria through the NADH shuttle system. By abolishing the NADH shuttle function, glucose-induced increases in NADH autofluorescence, mitochondrial membrane potential, and adenosine triphosphate content were reduced and glucose-induced insulin secretion was abrogated. The NADH shuttle evidently couples glycolysis with activation of mitochondrial energy metabolism to trigger insulin secretion.

Glucose metabolism through glycolysis in the cytosol and then through the tricarboxylic acid (TCA) cycle in mitochondria has been proposed to promote glucose-induced insulin secretion through generation of metabolic signals such as adenosine triphosphate (ATP) or an increase in the ratio of ATP to adenosine diphosphate (ADP) in pancreatic β cells (*1*). However, pyruvate, an end-product of aerobic glycolysis, fails to stimulate insulin secretion, although it can be oxidized in islets as efficiently as glucose (*2*). Studies with an inhibitor of pyruvate transport into mitochondria or an inhibitor of the TCA cycle suggest that metabolism of glucose-derived pyruvate in mitochondria or in the TCA cycle is not well correlated with glucose-induced insulin secretion (*3*). These findings imply that one or more factors derived from glycolysis other than pyruvate are required for the generation of mitochondrial signals that lead to insulin secretion. One candidate for these metabolic coupling factors is NADH generated by the glycolytic enzyme glyceraldehyde 3-phosphate dehydrogenase (GAPDH) (*4*). The cytosolic NADH is transferred into mitochondria for oxidative metabolism and ATP production through two NADH shuttles, the

[1]Department of Internal Medicine; [2]Department of Physiology; [3]Department of Pathology; [4]Department of Neurology, Graduate School of Medicine, University of Tokyo, 7-3-1 Hongo, Bunkyo-ku, Tokyo 113, Japan. [5]Department of Geriatrics, Endocrinology and Metabolism, Shinshu University School of Medicine, 3-1-1 Asahi, Matsumoto 390, Japan. [6]Institute for Diabetes Care and Research, Asahi Life Foundation, 1-6-1 Marunouchi, Chiyoda-ku, Tokyo 100, Japan. [7]Department of Morphogenesis, Institute of Molecular Embryology and Genetics, Kumamoto University School of Medicine, 4-24-1 Kuhonji, Kumamoto 862, Japan.

*To whom correspondence should be addressed. E-mail: kadowaki-3im@h.u-tokyo.ac.jp

glycerol phosphate shuttle (*5*) and the malate-aspartate shuttle (*6*).

To determine the role of the NADH shuttle system in glucose-induced insulin secretion, it may be necessary to inhibit both of the shuttles. We generated mice with a targeted disruption of mitochondrial glycerol 3-phosphate dehydrogenase (mGPDH) (*7*), a rate-limiting enzyme for the glycerol phosphate shuttle. By administration of aminooxyacetate (AOA), a well-characterized inhibitor of the malate-aspartate shuttle (*6, 8*), to mGPDH-deficient islets, we obtained a state in which the activities of both the shuttles were abolished. We then observed that the NADH shuttle system is essential for coupling glycolytic metabolism with activation of mitochondrial energy generation and thus for glucose-induced insulin secretion.

The absence of mGPDH protein in the islets from mice homozygous for the mutated *mGPDH* gene was confirmed by protein immunoblotting and by enzyme activity assay (*9*). The *mGPDH*$^{-/-}$ mice were fertile and had no gross abnormalities except for a small but significant impairment of body weight gain (*10*). The *mGPDH*$^{+/-}$ and *mGPDH*$^{-/-}$ mice were normoglycemic after overnight fasting and after feeding ad libitum, and both groups showed normal changes in blood glucose and serum insulin concentrations in an intraperitoneal glucose tolerance test (Fig. 1A) (*11*). In static incubation (*12*), wild-type, *mGPDH*$^{+/-}$, and *mGPDH*$^{-/-}$ islets secreted the same amounts of insulin in the presence of 2.8 or 22.2 mM glucose (Fig. 1B).

These results indicated that the other NADH shuttle, the malate-aspartate shuttle, might account for continued NADH transfer into mitochondria. We therefore administered AOA, an inhibitor of aspartate aminotransferase in the malate-aspartate shuttle, to islets. AOA (5 mM) suppressed aspartate aminotransferase activity in cytosolic fractions from wild-type and *mGPDH*$^{-/-}$ islets (3.3 ± 1.3% and 3.8 ± 2.4% of activities without AOA, respectively; $n = 4$) (*13*). In wild-type and *mGPDH*$^{+/-}$ islets, 5 mM AOA only slightly suppressed insulin release at 22.2 mM glucose (Fig. 1B). However, glucose-induced insulin release from *mGPDH*$^{-/-}$ islets treated with AOA was almost completely abolished, demonstrating that NADH shuttles are essential for glucose-induced insulin secretion. Perifusion experiments revealed that the first phase of glucose-induced insulin secretion from *mGPDH*$^{-/-}$ islets treated with AOA was severely suppressed and the second phase was completely abolished (Fig. 1C) (*14*). A similar severe reduction in insulin secretion was observed in response to 10 mM D-glyceraldehyde, which is metabolized by glycolysis and generates NADH in the cytosol (Fig. 1D). In contrast, *mGPDH*$^{-/-}$ islets with AOA responded normally to 10 μM glibenclamide, which bypasses mitochondrial metabolism and directly closes the ATP-sensitive potassium channel, or to 10 mM methyl pyruvate, which is metabolized solely within mitochondria, independent of NADH shuttles. These results demonstrate that NADH shuttles are required for the insulin secretory response to fuel molecules that are metabolized by glycolysis and trigger mitochondrial metabolism through the transfer of NADH.

We studied the metabolic fate of isotope-labeled glucose molecules under these conditions. According to the prevailing hypothesis, when both shuttles are halted, glycolysis

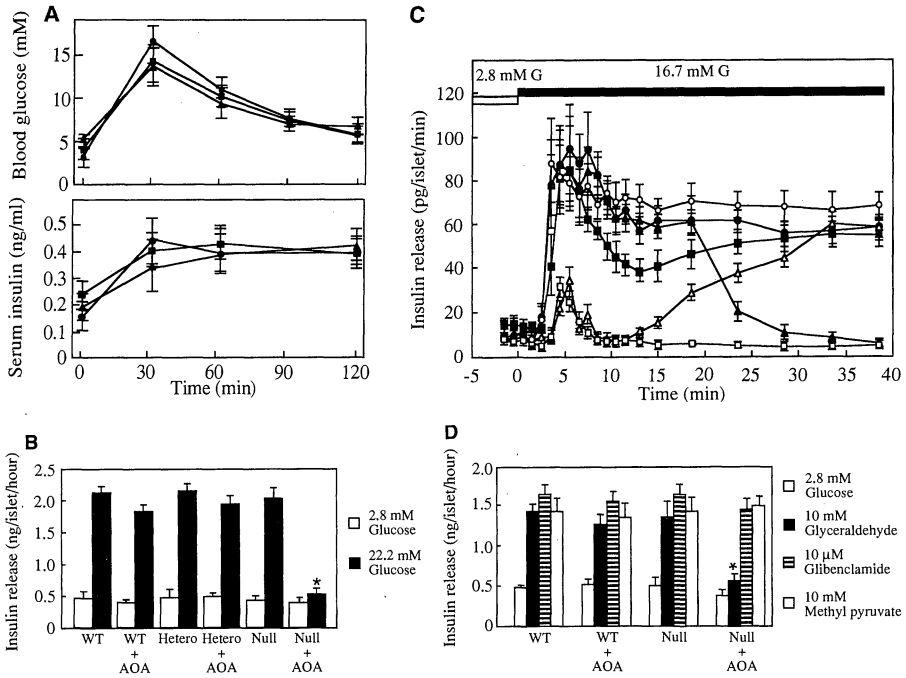

Fig. 1. Characteristics of insulin release by glucose and other secretagogues in mice and in islets. (**A**) Blood glucose profiles in a glucose tolerance test. Values were from wild-type (●, $n = 13$), *mGPDH*$^{+/-}$ (■, $n = 8$), and *mGPDH*$^{-/-}$ (▲, $n = 10$) mice. (**B**) Insulin release from islets in static incubation. Ten islets were incubated in buffer containing 2.8 or 22.2 mM glucose with or without 5 mM AOA. Data are from four to six independent experiments; *$P < 0.01$ as compared to wild-type controls (*28*). (**C**) Insulin release from islets in perifusion. Glucose (G) concentration was raised from 2.8 to 16.7 mM at 0 min. Data are from four to six independent experiments with islets from wild-type mice treated without (●) or with 5 mM AOA (■), or from *mGPDH*$^{-/-}$ mice treated without (○) or with 5 mM AOA (□), with 5 mM AOA that was added to buffer at 15 min (▲), or with 5 mM AOA that was removed from buffer at 10 min (△). (**D**) Insulin release from islets in response to 10 mM D-glyceraldehyde, 10 μM glibenclamide, or 10 mM methyl pyruvate in static incubation; *$P < 0.01$ as compared to wild-type controls (*28*).

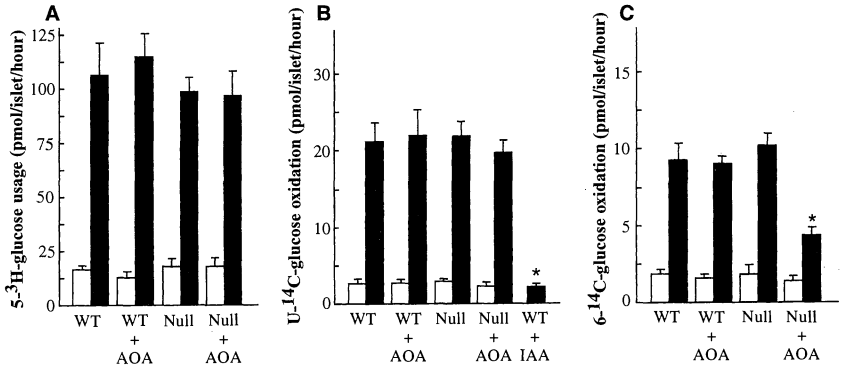

Fig. 2. Glucose usage in glycolysis and glucose oxidation in mitochondria and in the TCA cycle. Ten islets were incubated at 37°C for 1 hour in buffer containing 2.8 mM (open bars) or 22.2 mM glucose (solid bars) with or without 5 mM AOA. Data are from four to six independent experiments; *$P < 0.01$ as compared to wild-type controls (*28*). (**A**) [5-^{3}H]glucose usage in glycolysis, as assayed by measurement of $[^3H]H_2O$ production. (**B**) [U-^{14}C]glucose oxidation in mitochondria, as assayed by measurement of $[^{14}C]CO_2$ production. (**C**) [6-^{14}C]glucose oxidation in the TCA cycle, as assayed by measurement of $[^{14}C]CO_2$ production.

should also be halted by depletion of the oxidized form of nicotinamide adenine dinucleotide (NAD^+) required for the reaction catalyzed by GAPDH (*5, 6*). However, glucose usage in glycolysis, measured by $[^3H]H_2O$ production from $[5\text{-}^3H]H_2O$, was not affected in *mGPDH*$^{-/-}$ islets incubated with 5 mM AOA (Fig. 2A). Moreover, oxidation of [U-^{14}C]glucose in *mGPDH*$^{-/-}$ islets with AOA was not significantly different from that in wild-type islets (Fig. 2B). Administration of 1 mM monoiodoacetic acid (IAA), an inhibitor of GAPDH, to wild-type islets completely suppressed oxidation of [U-^{14}C]glucose. These results indicated that production of pyruvate from glucose via glycolysis and transport of the glucose-derived pyruvate into mitochondria for oxidation were not significantly affected even when both shuttles were halted.

We thus hypothesized that the abolition of insulin secretion observed in *mGPDH*$^{-/-}$ islets treated with AOA was caused not by an insufficient supply of pyruvate to mitochondria but by a halt of NADH supply to mitochondria. To assess the contribution of the TCA cycle to glucose oxidation, we also measured [6-^{14}C]glucose oxidation (*15*). In the presence of 5 mM AOA, [6-^{14}C]glucose oxidation in *mGPDH*$^{-/-}$ islets was decreased by 58% at 22.2 mM glucose relative to that in wild-type islets (Fig. 2C).

To explore the potential mechanism by which TCA cycle activity was impaired in the absence of NADH shuttles, we monitored the autofluorescence of the reduced form of nicotinamide adenine dinucleotide (phosphate) [NAD(P)H] (*16*). These signals are thought to originate from the mitochondrial pool of NADH (*17*). In *mGPDH*$^{-/-}$ islets (Fig. 3C) or in wild-type islets treated with 5 mM AOA (Fig. 3B), the increase in autofluorescence in response to 22.2 mM glucose (28.4 ± 2.2% and 23.8 ± 3.1%, respectively) was not different from that in wild-type islets (27.1 ± 3.8%) (Fig. 3A). However, the increase in AOA-treated *mGPDH*$^{-/-}$ islets was attenuated to a rise of only 7.2 ± 1.3% (Fig. 3D). These amounts of NAD(P)H were well correlated with the extent of mitochondrial membrane hyperpolarization measured by fluorescence of Rhodamine 123 (Rh123) (*18*). In *mGPDH*$^{-/-}$ islets (Fig. 3G) or AOA-treated wild-type islets (Fig. 3F), the decrease in Rh123 fluorescence in response to 22.2 mM glucose (28.0 ± 4.0% and 22.8 ± 1.4%, respectively) was comparable to that in wild-type islets (28.4 ± 4.3%) (Fig. 3E). In AOA-treated *mGPDH*$^{-/-}$ islets, however, the decrease was attenuated to a drop of only 7.9 ± 0.8% (Fig. 3H). The ATP content and ATP/ADP ratio in islets were significantly decreased at 22.2 mM glucose in AOA-treated *mGPDH*$^{-/-}$ islets relative to those of wild-type islets (Table 1) (*19*). The glucose-responsive increase in ATP content of AOA-treated *mGPDH*$^{-/-}$ islets was reduced to 38% of that of wild-type islets. The ATP content measured in this manner contained glycolysis-derived ATP, which was assumed to be unaffected under these conditions, and ATP sequestered in a metabolically inert pool, which corresponds to ~30% of cellular ATP (*20*). Moreover, the insulin secretory processes themselves consume large amounts of ATP

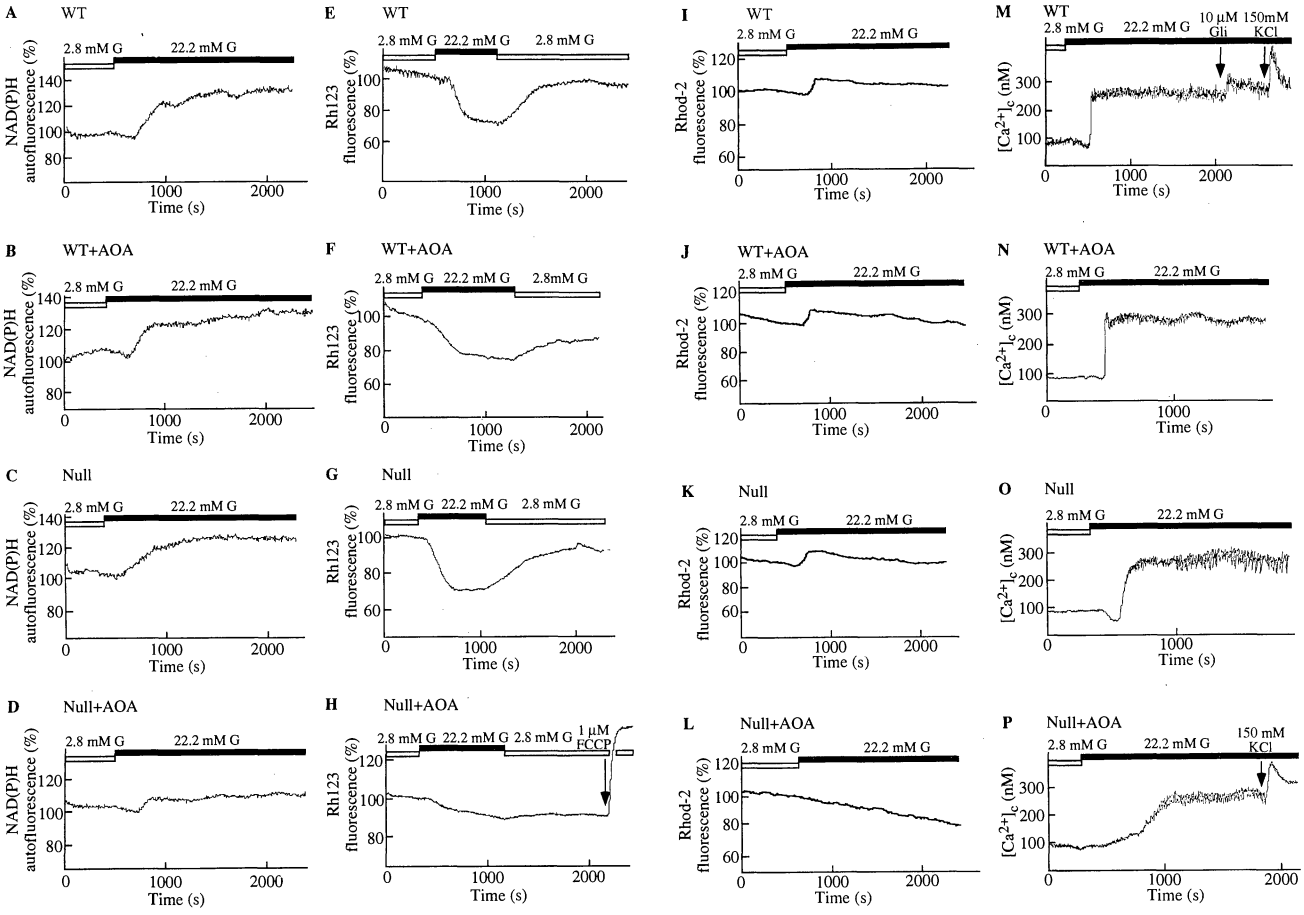

Fig. 3. Glucose-induced changes of metabolic parameters in mitochondria and $[Ca^{2+}]$ in mitochondria and cytosol. Representative traces from at least six experiments are shown in each panel. Glucose (G) concentrations in perifusate were raised to 22.2 mM and lowered to 2.8 mM at the indicated time points. (**A** to **D**) Profiles of NAD(P)H autofluorescence. (**E** to **H**) Profiles of Rh123 fluorescence to monitor mitochondrial membrane potential. Downward changes indicate hyperpolarization. The mitochondrial electron transport uncoupler carbonyl cyanide *p*-(trifluoromethoxy)phenyl-hydrazone (FCCP) (1 μM) was applied in (H). (**I** to **L**) Profiles of Rhod 2 fluorescence to monitor $[Ca^{2+}]_m$. (**M** to **P**) Profiles of Fura 2 fluorescence to monitor $[Ca^{2+}]_c$. Application of 10 μM glibenclamide (Gli) (M) or 150 mM KCl (M and P) further elevated $[Ca^{2+}]_c$.

in wild-type islets but not in AOA-treated *mGPDH*$^{-/-}$ islets. Therefore, the glucose-responsive increase in mitochondrial ATP generation is estimated to be more severely affected than these results might indicate. Collectively, NADH shuttles appear to have a major regulatory role in the activation of β cells' mitochondrial energy metabolism in response to glucose.

The intramitochondrial concentration of Ca^{2+} ($[Ca^{2+}]_m$) rises in parallel with the concentration of cytoplasmic Ca^{2+} ($[Ca^{2+}]_c$) in response to glucose stimulation and is closely linked to insulin release (*21*). Ca^{2+} entry into mitochondria is mediated through a Ca^{2+} uniporter on the inner membrane, the activity of which is dependent on change in mitochondrial membrane potential (*22*). To test whether the reduced hyperpolarization of mitochondrial membrane potential in response to glucose observed in AOA-treated *mGPDH*$^{-/-}$ islets was insufficient to activate the Ca^{2+} uniporter, we used Rhod 2 to measure $[Ca^{2+}]_m$ (*23*). The increase in Rhod 2 fluorescence in *mGPDH*$^{-/-}$ islets (Fig. 3K) or wild-type islets treated with 5 mM AOA (Fig. 3J) in response to 22.2 mM glucose (11.9 ± 3.4% and 10.5 ± 2.1%, respectively) was not significantly different from that in wild-type islets (12.2 ± 2.9%) (Fig. 3I). However, in AOA-treated *mGPDH*$^{-/-}$ islets, no increase in Rhod 2 fluorescence was observed (0.5 ± 0.4%) (Fig. 3L). Thus, the glucose-induced increase in $[Ca^{2+}]_m$ is under the influence of NADH transfer via the shuttles. Abolition of the rise in $[Ca^{2+}]_m$ may impair the activation of intramitochondrial Ca^{2+}-dependent dehydrogenases (*24*), and thus may explain (at least in part) the attenuated feedforward activation of the TCA cycle by glucose. Responses of $[Ca^{2+}]_c$ were also monitored by Fura 2 fluorescence (*25*). In *mGPDH*$^{-/-}$ islets (Fig. 3O), a normal $[Ca^{2+}]_c$ response to 22.2 mM glucose was observed: an initial dip and subsequent sharp rise (first phase) followed by a sustained plateau (second phase), as was observed in wild-type islets (Fig. 3M). Wild-type islets treated with 5 mM AOA also showed a normal response (Fig. 3N). In *mGPDH*$^{-/-}$ islets treated with AOA, however, the initial dip and the first-phase peak did not occur. Still, $[Ca^{2+}]_c$ gradually reached the second phase in 10 to 15 min, which was comparable in amplitude to that observed in wild-type islets (Fig. 3P). Thus, the rise in $[Ca^{2+}]_c$ and insulin secretion appeared not to be coupled in the absence of functional NADH shuttles (compare Figs. 1C and 3P).

We construe the dissociation between the $[Ca^{2+}]_c$ rise and the inhibited insulin secretion as follows. First, a marked reduction in ATP generation may not provide sufficient energy for the movement of secretory granules toward the plasma membrane, for priming of the exocytosis machinery, or for the final fusion process of secretory granules (*1*). Second, the time course of $[Ca^{2+}]_c$ rise to the second-phase plateau was disordered. The disappearance of the initial dip and the first-phase rise of $[Ca^{2+}]_c$ suggests that Ca^{2+} uptake of endoplasmic reticulum by Ca^{2+}–adenosine triphosphatase and Ca^{2+} influx through voltage-dependent Ca^{2+} channels from the extracellular compartment are severely impaired (*26*). Thus, the $[Ca^{2+}]_c$ rise may not take place at the time and site that are critical for exocytosis.

We tested whether the 58% decrease in the activity of the TCA cycle alone in *mGPDH*$^{-/-}$ islets treated with AOA might be sufficient to abolish insulin secretion. However, when glucose oxidation in the TCA cycle was inhibited with monofluoroacetic acid (an inhibitor of the TCA cycle enzyme aconitase) by 48 to 62% in wild-type islets, glucose-induced increases in NAD(P)H autofluorescence, mitochondrial membrane potential, $[Ca^{2+}]_m$, and ATP content were largely unaffected and insulin secretion was completely retained (*27*), consistent with previous results (*3*). Thus, the activity of the TCA cycle alone appears not to account for the abolition of glucose-induced insulin secretion. Rather, the halt of the NADH shuttle system itself may be the cause.

Glucose is thought to be metabolized to pyruvate in aerobic glycolysis, and the subsequent oxidation of pyruvate in the TCA cycle is thought to almost exclusively provide the mitochondrial NADH and the reduced form of flavin adenine dinucleotide ($FADH_2$) (Fig. 4A). In contrast to this hypothesis, inhibition of both shuttles was associated with the suppression of glucose-induced increases in NAD(P)H autofluorescence, mitochondrial membrane potential, and mitochondrial ATP content to 25 to 30% of the normal state, and insulin secretion was abolished. Abolition of the NADH shuttle system resulted in a ~50% reduction of the TCA cycle activity, so contributions of the TCA cycle and NADH shuttle system to mitochondrial ATP production may be approximately equal in the physiological state. Thus, we propose an alternative model for metabolic phases of glucose-induced insulin secretion (Fig. 4B). Glucose stimulation of β cells can both produce NADH in the cytosol and provide pyruvate for the TCA cycle. Cytosolic

Table 1. ATP content and ATP/ADP ratio in glucose-stimulated islets. Islets were incubated at 2.8 or 22.2 mM glucose at 37°C for 1 hour, and the metabolism was snap-stopped by addition of ice-cold 1N perchloric acid and liquid nitrogen freezing. After thawing, samples were sonicated and neutralized with NaOH. ATP and ADP contents were measured with a luciferase-luciferin system (*19*). Data are from six to eight independent experiments; *$P < 0.01$ as compared to wild-type islets (*28*).

Glucose	WT	WT + AOA	Null	Null + AOA
		ATP (picomoles per islet)		
2.8 mM	8.03 ± 0.36	8.11 ± 0.26	7.50 ± 0.67	7.38 ± 0.36
22.2 mM	13.32 ± 1.06	13.24 ± 0.94	12.72 ± 0.39	9.41 ± 0.51*
		ATP/ADP ratio		
2.8 mM	2.24 ± 0.29	2.49 ± 0.27	2.56 ± 0.35	2.36 ± 0.30
22.2 mM	5.41 ± 0.41	4.96 ± 0.44	5.07 ± 0.28	3.17 ± 0.34*

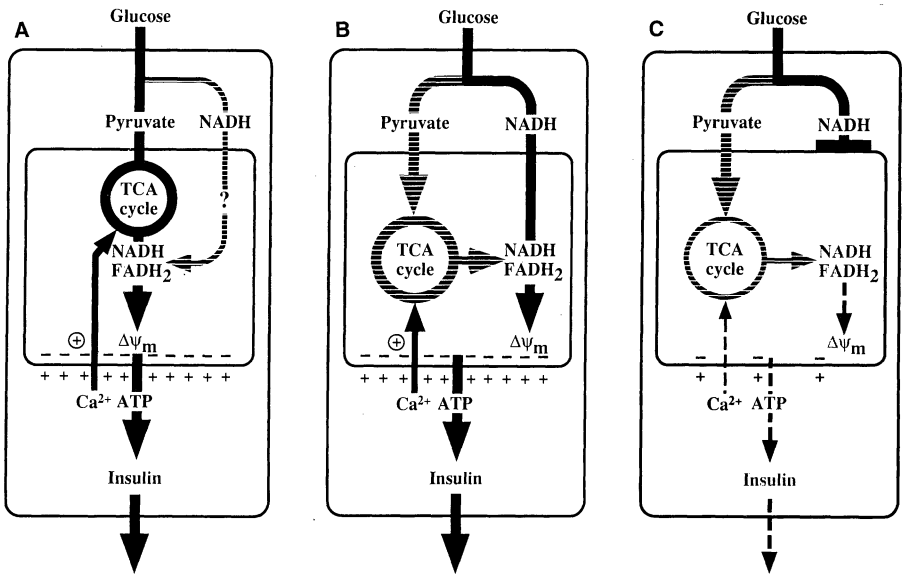

Fig. 4. Schematic models for classical and alternative pathways of glucose-induced insulin secretion in β cells. (**A**) A classical model. (**B**) The alternative model. (**C**) Alternative model when both NADH shuttles are halted.

NADH can be transferred into mitochondria through the NADH shuttles, and concomitantly it leads to an increase in $[Ca^{2+}]_m$ after the formation of mitochondrial membrane potential, thereby activating pyruvate oxidation in the TCA cycle. The NADH shuttles thus would contribute to sufficient ATP generation to trigger glucose-induced insulin secretion. When NADH shuttles are halted, the activity of the TCA cycle is also decreased by ~50%, at least in part because of concurrent inhibition of Ca^{2+} entry into mitochondria. The resultant severe decrease in mitochondrial ATP synthesis to ~25% of the normal state no longer maintains glucose-induced insulin secretion (Fig. 4C). Thus, defects in the generation of mitochondrial metabolic signals through the NADH shuttles might contribute to the impairment of glucose-induced insulin secretion seen in non–insulin-dependent diabetes mellitus.

References and Notes

1. F. M. Ashcroft *et al.*, *J. Cell Biochem.* **55** (suppl.), 54 (1994); F. M. Matschinsky, *Diabetes* **45**, 223 (1996); C. B. Wollheim *et al.*, *Diabetes Rev.* **4**, 276 (1996).
2. A. Sener *et al.*, *Biochem. J.* **176**, 217 (1978); W. S. Zawalich and K. C. Zawalich, *J. Biol. Chem.* **272**, 3527 (1997).
3. I. D. Dukes *et al.*, *J. Biol. Chem.* **269**, 10979 (1994); R. J. Mertz *et al.*, *ibid.* **271**, 4838 (1996).
4. W. J. Malaisse *et al.*, *Metabolism* **28**, 373 (1979); C. J. Hedeskov *et al.*, *Biochem. J.* **241**, 161 (1987); W.-F. Pralong *et al.*, *EMBO J.* **9**, 53 (1990).
5. M. J. MacDonald, *J. Biol. Chem.* **256**, 8287 (1981).
6. ———, *Arch. Biochem. Biophys.* **213**, 643 (1982).
7. A BALB/c mouse *mGPDH* gene containing exons 4, 5, and 6 was cloned and a neomycin resistance gene under transcriptional control of the mouse phosphoglycerate kinase–1 promoter (PGK-neo) was inserted within exon 5. The 8.1 kb (5′) and 1.7 kb (3′) of genomic DNA flanking PGK-neo was ligated into a pMCDT-A plasmid (Gibco-BRL) that produces diphtheria toxin A fragment for negative selection. The completed targeting vector was linearized and electroporated into TT2 embryonic stem cells. The cells were cultured with G418. The choice of targeted clones was based on the shift of a genomic fragment by Pvu II digestion from 3.4 to 3.1 kb, as determined by Southern (DNA) blot. Targeted embryonic stem cells were injected into blastocytes from C57BL/6J mice to sequentially obtain chimeric, heterozygous, and homozygous offspring. All the mice used were males from heterozygous breeding pairs. All islets were from 16- to 20-week-old mice.
8. W. J. Malaisse *et al.*, *Endocrinology* **111**, 392 (1982).
9. Antibody to mGPDH was raised against the COOH-terminal sequence Lys-Thr-Ala-Glu-Glu-Asn-Leu-Asp-Arg-Arg-Val-Pro-Ile-Pro-Val-Asp-Arg-Ser-Cys-Gly-Gly-Leu. Islets were isolated by collagenase digestion and homogenated in 0.23 M mannitol, 0.07 M sucrose, and 5 mM Hepes (pH 7.5). Activities of mGPDH were measured as described [R. S. Gardner, *Anal. Biochem.* **59**, 272 (1974)].
10. Relative to wild-type controls, male and female $mGPDH^{-/-}$ mice at 16 weeks of age were smaller by 23% and 13%, respectively. Relative to wild-type islets, $mGPDH^{-/-}$ islets had normal cellular architecture and contained approximately the same amounts of insulin and glucagon.
11. For the glucose tolerance test, glucose (1.5 mg/g body weight) was injected into the peritoneum. Blood samples were drawn from tail veins.
12. Insulin secretion was measured with Krebs-Ringer-bicarbonate buffer containing 118.4 mM NaCl, 4.7 mM KCl, 1.3 mM $MgSO_4$, 1.2 mM KH_2PO_4, 2.0 mM $CaCl_2$, 10 mM $NaHCO_3$, 10 mM Hepes (pH 7.4), and 0.1% bovine serum albumin at 37°C. Basal glucose concentration was 2.8 mM, and AOA was added to buffer during preincubation (30 min) and throughout the incubation period unless otherwise stated.
13. Islet homogenates were centrifuged at 600*g* for 5 min and the supernatant was centrifuged at 5500*g* for 10 min to sediment the mitochondrial fraction. The resulting supernatant was used as the cytosolic fraction.
14. Perifusion experiments were done with 30 islets per chamber at 37°C with a flow rate of 0.6 ml/min.
15. F. Schuit *et al.*, *J. Biol. Chem.* **272**, 18572 (1997).
16. For fluorescence studies, a single islet was placed under a microscope (IMT-2; Olympus, Japan) and perifused with buffer containing 150 mM NaCl, 5 mM KCl, 1.0 mM $MgCl_2$, 2.0 mM $CaCl_2$, and 10 mM Hepes (pH 7.4) at 37°C. Fluorescence was excited with light emitted from a xenon lamp (TILL Photonics, Germany), collected through interference filters (Olympus), and detected using a photomultiplier (NT5783; Hamamatsu Photonics, Japan). NAD(P)H was measured by autofluorescence excited at 360 nm and filtered at 470 nm.
17. M. R. Duchen *et al.*, *Biochem. J.* **294**, 35 (1993).
18. For measurement of mitochondrial membrane potential, islets were loaded with Rh123 (10 μg/ml, Sigma) at 37°C for 10 min. The fluorescence was excited at 490 nm and filtered at 530 nm as described [P. Maechler *et al.*, *EMBO J.* **16**, 3833 (1997)].
19. W. J. Malaisse and A. Sener, *Biochim. Biophys. Acta* **927**, 190 (1987).
20. M. Erecinska *et al.*, *ibid.* **1101**, 273 (1992).
21. E. D. Kennedy *et al.*, *J. Clin. Invest.* **98**, 2524 (1996).
22. M. L. Litsky and D. R. Pfeiffer, *Biochemistry* **36**, 7071 (1997).
23. For measurement of $[Ca^{2+}]_m$, islets were loaded with 10 μM Rhod 2/acetoxymethylester (Molecular Probes) at 37°C for 1 hour and further incubated for 3 to 5 hours to eliminate the dye from cytosol [G. Hajnóczky *et al.*, *Cell* **82**, 415 (1995); D. R. Trollinger *et al.*, *Biochem. Biophys. Res. Commun.* **236**, 738 (1997)]. The fluorescence was excited at 480 nm and filtered at 500 nm.
24. T. E. Gunter *et al.*, *Am. J. Physiol.* **267**, C313 (1994).
25. For measurement of $[Ca^{2+}]_c$, islets were loaded with 15 μM Fura 2/acetoxymethylester (Molecular Probes) at 37°C for 1 hour. The fluorescence was excited alternately at 340 and 380 nm and filtered at 500 nm.
26. N. Hamakawa and T. Yada, *Cell Calcium* **17**, 21 (1995); F. M. Ashcroft *et al.*, *Nature* **312**, 446 (1984).
27. K. Eto *et al.*, unpublished data.
28. Results are presented as means ± SE. The significance of the differences between groups was determined using one-way analysis of variance.

29. We thank C. B. Wollheim and F. M. Ashcroft for invaluable discussion, Y. Kagawa, H. Sakura, M. Noda, and K. Yasuda for critical reading of the manuscript, and N. Takeda, M. Nagai, H. Yajima, C. Sato, H. Chiyonobu, and J. Taka for support. Supported by a grant-in-aid for creative basic research (10NP0201) from the Ministry of Education, Science, Sports, and Culture of Japan (T.K.) and by CREST of the Japan Science and Technology Corporation (H.K.).

25 August 1998; accepted 12 January 1999

Conserved Structures of Mediator and RNA Polymerase II Holoenzyme

Francisco J. Asturias,* Yi Wei Jiang, Lawrence C. Myers, Claes M. Gustafsson,† Roger D. Kornberg‡

Single particles of the mediator of transcriptional regulation (Mediator) and of RNA polymerase II holoenzyme were revealed by electron microscopy and image processing. Mediator alone appeared compact, but at high pH or in the presence of RNA polymerase II it displayed an extended conformation. Holoenzyme contained Mediator in a fully extended state, partially enveloping the globular polymerase, with points of apparent contact in the vicinity of the polymerase carboxyl-terminal domain and the DNA-binding channel. A similarity in appearance and conformational behavior of yeast and murine complexes indicates a conservation of Mediator structure among eukaryotes.

Mediator was isolated as a complex of nearly 20 proteins required to support transcriptional activation in a fully reconstituted yeast RNA polymerase II transcription system (*1, 2*). Mediator subunits fall into three groups: Srb proteins (*3*), a Sin4/Rgr1 group shown to form a distinct module that functions in repression as well as in activation (*4, 5*), and a group of proteins termed "Med" for Mediator (*5*). A related complex, containing four homologs of yeast Mediator subunits, has been isolated from murine cells (*6*). Yeast and murine complexes interact with RNA polymerase II through the polymerase's COOH-terminal domain (CTD) to form a 1.5-MD holoenzyme (*2, 3, 5*). We report here on the structures of Mediator and the holoenzyme as seen in projection.

Yeast Mediator, resolved to homogeneity as described (*7, 8*), was adsorbed to carbon-coated grids and negatively stained with uranyl acetate for imaging in the electron microscope. Fields of many similar particles were observed, which suggests that Mediator exists as a discrete entity, as was previously inferred from biochemical studies. A large fraction of the particles appeared to be nearly identical, which is indicative of a preferred orientation on the grid (*9*).

Department of Structural Biology, Fairchild Building, Stanford University School of Medicine, Stanford, CA 94305, USA.

*Present address: Department of Cell Biology MB 25, The Scripps Research Institute, 10550 North Torrey Pines Road, La Jolla, CA 92037, USA.

†Present address: Institute of Medical Biochemistry, Göteborg University, Medicinaregatan 13, 405 30 Göteborg, Sweden.

‡To whom correspondence should be addressed. E-mail: kornberg@stanford.edu